Helicopter Non-Unique Trim Strategies for Blade-Vortex Interaction (BVI) Noise Reduction

Carlos Malpica
Aerospace Engineer
NASA Ames Research Center
Moffett Field, CA

Eric Greenwood
Aerospace Engineer
NASA Langley Research Center
Hampton, VA

Ben W. Sim
Research Engineer
US Army Aviation Development Directorate
Moffett Field, CA

ABSTRACT

An acoustics parametric analysis of the effect of fuselage drag and pitching moment on the Blade-Vortex Interaction (BVI) noise radiated by a medium lift helicopter (S-70/UH-60) in a descending flight condition was conducted. The comprehensive analysis CAMRAD II was used for the calculation of vehicle trim, wake geometry and integrated air loads on the blade. The acoustics prediction code PSU-WOPWOP was used for calculating acoustic pressure signatures for a hemispherical grid centered at the hub. This paper revisits the concept of the *X*-force controller for BVI noise reduction, and investigates its effectiveness on an S-70 helicopter. The analysis showed that further BVI noise reductions were achievable by controlling the fuselage pitching moment. Reductions in excess of 6 dB of the peak BVI noise radiated towards the ground were demonstrated by compounding the effect of airframe drag and pitching moment simultaneously.

INTRODUCTION

Background

High levels of harmonic rotor noise are one of the key technical barriers preventing the widespread public acceptance of helicopters for commercial transportation. Blade-Vortex Interaction (BVI) is one such mechanism of rotor noise. BVI noise is a problem for civilian helicopter terminal area operations because the noise occurs itself primarily in descending flight, with the peak noise signatures occurring near the standard 6 degree glide path angle on approach.

Joint NASA/Army research programs, including wind tunnel and flight testing, have identified technologies that could offer significant noise reductions through careful management or control of the approach flight path profile or by means of active rotor control systems directly affecting the blade loading. Active rotor control, such as with Individual Blade Control (using blade root-actuated systems in Ref. 1 and active flaps in the case of Ref. 2) has been shown to be effective in reducing both types of noise, (but at the expense of increasing the vibratory N/rev loads). In the case of harmonic, low-frequency in-plane noise, reduction of the acoustic signature strength was achieved through the superposition of acoustic pulses generated by the blade air loads on the advancing side of the rotor in such a manner that attenuated the negative pressure peaks associated with the in-plane, steady thickness noise (Ref. 2). These techniques, however, are either operationally impractical, or largely remain in an experimental status, not yet meeting the airworthiness standards required for certification.

An alternative approach is to exploit the net effect of aerodynamic surfaces (on the fuselage, in the non-rotating frame) on the vehicle trim which in turn affects noise generation. For example, conventional single main rotor helicopters commonly employ fixed-incidence, horizontal stabilizers to generate auxiliary aerodynamic forces to enhance stability about pitch. More advanced rotorcraft designs incorporate a variable incidence stabilator that is set automatically by the on-board flight control computer using airspeed and other measurements. Such a device has resulted in reduced downloads at hover, and has also enabled operation at favorable fuselage attitudes that minimize drag to achieve better cruise performance. These types of devices offer the potential to alter source noise by manipulating vehicle trim.

This basic idea is at the heart of the so-called *X*-force control concept proposed in Ref. 3 for BVI noise reduction. The research of Ref. 4 showed that flying decelerating approaches could affect BVI noise by altering the rotor tip-path-plane angle of attack and wake geometry. The underpinning mechanism was the increased longitudinal (propulsive) trim force (the rotor *X*-force) obtained in a decelerating approach, which was sufficient to tilt the rotor tip-path-plane forward enough to provide an appreciable reduction in the BVI noise. The same fundamental principles were successfully tested on the XV-15 tiltrotor in Ref. 5.

Presented at the AHS Technical Meeting on Aeromechanics Design for Vertical Lift, January 20–22, 2016.

Objective

The primary goal of this study is to establish the feasibility of *X*-force control, for a medium- to heavy-lift single main rotor helicopter, by investigating the sensitivity of BVI noise radiation to changes in the trim state of the rotor. The coupled effect of fuselage pitching moment will also be investigated.

Technical Approach

The use of an air brake, or other drag device, on the fuselage is proposed in order to indirectly affect the propulsive trim force and manipulate the tilt of the rotor tip-path-plane during a descending approach. Other types of control surfaces, such as stabilators, are already used in some helicopters. Their availability and the significant effect on the vehicle airloads in trim makes the stabilator an intriguing option for BVI noise control. It is therefore of interest to also assess its influence on rotor acoustics. This is made more so due to the coupled nature of the propulsive force and pitch.

Analysis of the subject rotor and vehicle configurations was performed with the comprehensive rotorcraft aeromechanics analysis CAMRAD II (Ref. 6). Acoustics predictions were performed primarily using the PSU-WOPWOP analysis (Ref. 7) and other in-house acoustics prediction codes. Ideally, this comparative, parallel analysis will prove to yield more conclusive results.

The S-70 helicopter was chosen for this study as a proxy to the S-92 HELIBUS due to the similarities of their rotors. The S-92 is of particular interest because of its potential use as a commercial transport. The S-92 and similarly sized helicopters are used extensively for civilian operations, mainly for transporting crew and equipment to offshore oil rigging facilities, but with a 19-passenger approximate capacity, they are well suited to a short-range commercial airliner market.

The S-70 main rotor blade has similar characteristics to the S-92, including improved airfoil design and blade tip configuration (swept, tapered and anhedral tip), as well as a fully composite material spar. The S-70 blade, however, is narrower and has a shorter radius than the S-92 helicopter. Instrumented UH-60/S-70 rotors have been the subject of numerous wind tunnel and flight tests conducted by NASA and the U.S. Army. This choice therefore offers a wide source of aerodynamic and acoustic data measurements for model validation.

ANALYTICAL MODEL

Acoustics prediction methodology

Rotor noise predictions are derived from blade geometry and predicted blade airloads. The latter is obtained from the comprehensive rotor analysis CAMRAD-II which models the blade structural properties, rotor wake geometry, and local unsteady blade aerodynamics. Within the analysis, blade modeling is based on a series of span-wise distributed nonlinear beam finite elements. Each beam element is represented by a full range of blade motions, which includes axial, lead-lag, flapping and torsion. A non-uniform inflow model coupled to a free wake is used to obtain aerodynamic forces and blade motion solutions that satisfy the rotor thrust, propulsive force and pitch/roll moments required for the full vehicle free flight trim condition.

In all ensuing calculations, the rotor blade is modeled using twenty aerodynamic panels on each blade. The panels are more densely distributed at the outboard (tip) region of the rotor blade to accurately simulate the dominant region important for sound radiation. Steady airloads are computed using C-81 airfoil tables. Unsteady lift and moment in the attached flow are calculated based on compressible thin-airfoil theory. For vehicle trim calculations the aerodynamic loads on the blades are evaluated at azimuth intervals of 15 deg. The relatively large time (azimuth) step is adequate for capturing low frequency sound, but BVI noise calculation requires a time (azimuth) step of 1 deg or smaller, to capture higher frequency content. An azimuthal resolution of 1 deg was used in this study. CAMRAD II generates this fine azimuthal resolution after achieving a converged trim solution, by reconstructing the wake geometry and blade motion at the intermediate azimuths.

As previously indicated, PSU-WOPWOP, primarily, was used to generate the rotor BVI noise predictions. The code uses blade planform/airfoil geometry, and pre-determined aerodynamic loading to resolve rotor acoustics radiation in the time-domain, based on Farassat's Formulation 1A (Ref. 8). The noise is computed for any observer in both the near and the far-field. For this study, PSU-WOPWOP was specifically configured to make use of the CAMRAD-II-derived blade motion and its resulting unsteady airloads.

A hemispherical observer grid, centered at the rotor hub, was configured for the calculation of acoustic pressures. Observers were placed at azimuthal intervals of 20 degrees and elevation intervals of 12.5 deg starting from the horizon down to 75 deg. One additional observer was placed directly below the hub. The radial distance of the observers from the hub was 500 ft. The observer grid was aligned to the inertial reference frame but forced to translate along with the vehicle.

The BVI Sound Pressure Level (BVI SPL) metric used throughout this paper to characterize the BVI noise was calculated in PSU-WOPWOP by integrating the sound pressure power spectra between the 10^{th} and 50^{th} blade passage harmonics. For a nominal rotor speed of 27 rad/s, these band-pass filter frequencies corresponded to 172 and 860 Hz, approximately.

Model calibration. One of the challenges of conducting analytical acoustics predictions using compact-chord models with integrated airloads (instead of surface pressures), such

as those obtained from a comprehensive code like CAMRAD, is that loading noise tends to be over-predicted (Ref. 9). Typically a 6 dB over-prediction is to be expected. Furthermore, these calculations tend to be quite sensitive to the wake model tip vortex core size. The analytical model employed for the acoustic predictions was therefore calibrated to the measured BVI amplitude from the full-scale UH-60A main rotor wind tunnel test (Ref. 10) by adjusting the tip vortex core size. Predictions from two analytical acoustics codes for 40, 80, 120 and 160% (relative to the chord length) free-wake model tip vortex core sizes are compared to the wind tunnel data in Figure 1. Further comparison for the calibrated model are shown in Figure 2. The results shown in Figure 2 confirm the coupled CAMRADII/PSU-WOPWOP analytical models adequately capture, or represent, the fundamental governing relationship between BVI noise and aerodynamic angle of attack of the rotor.

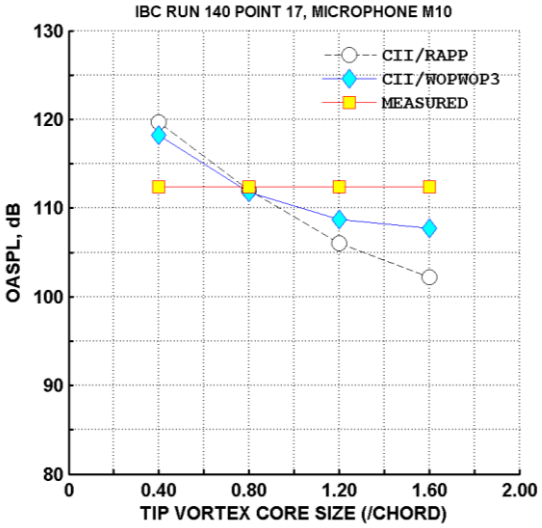

(a)

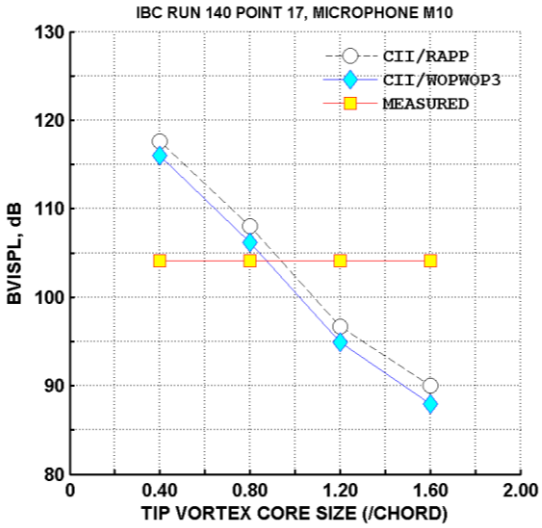

(b)

Figure 1. Sensitivity of rotor acoustics to wake model tip vortex strength: (a) OASPL and (b) BVISPL

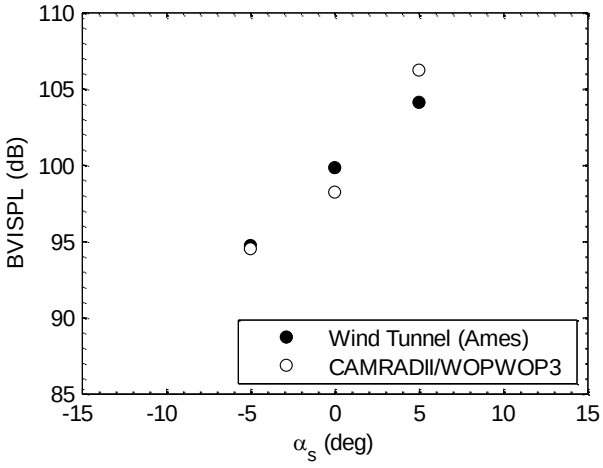

Figure 2. Comparison of acoustic predictions and wind tunnel BVI measurements (80% tip vortex core radius)

Helicopter configuration

The CAMRAD II S-70/UH-60 helicopter model used was based on Ref. 11. The model consisted of a single main rotor and a tail rotor. An aerodynamic interference model in CAMRAD II was used. This model relied on a uniform inflow approximation to compute the main rotor wake interference effects at collocation points off the rotor: wing-body, horizontal tail, vertical tail, and tail boom.

The trim solution in CAMRAD II was computed for a vehicle gross weight configuration of 18,500 lb, at a flight speed of 80 knots and a descent flight path angle of 6 deg. The nominal operating rotor speed was 258 rpm (27.0 rad/s). Atmospheric conditions were chosen for a standard day and an altitude of 1000 ft. Consequently, the air density and temperature were calculated at 0.002308 slug/ft^3 and 55.4 F, respectively. Given these conditions, CAMRAD II solves for the controls and aircraft attitudes that balance the forces and moments with zero sideslip angle and 6 deg descent.

Fuselage aerodynamics. Omitting the contributions from flap, flaperon or elevator control surfaces, the fuselage aerodynamic moment and drag in CAMRAD II were given as:

$$\frac{M_y}{q} = \frac{M_0}{q} + \frac{28.0}{q}\left(\alpha_F - 1.43\right)$$

$$\frac{D}{q} = \frac{D_0}{q} + 0.016\left(\frac{L}{q}\right)^2 = \frac{D_0}{q} + 0.016\left(1.66\alpha_F\right)^2$$

where q is the dynamic pressure and α_F is the fuselage aerodynamic angle of attack in degrees. The stabilator and vertical tail contribute additional aerodynamic loads. The stabilator angle of attack was set to -7.5 deg for the flight condition, based on measurements taken from the UH-60A Airloads Program (Refs. 12 and 13). The value of the drag

and the pitching moment at zero angle of attack are varied parametrically as shown in Table 1.

Table 1. Parametric drag and moment configurations

$f = D_0/q$ (ft^2)	M_0/q (ft^3)
26.2	
36.4	
46.6	0
67.0	
87.4	
	-400
	-200
	0
36.4	200
	400
	800
	1,600

RESULTS

Peak BVI Sound Pressure Level (SPL)

The effect of the change in fuselage drag on the peak BVI noise, at a distance of 500 ft from the main rotor hub, is shown in Figure 3. Overall, a 5.3 dB total reduction is attained by increasing the flat plate area for a "clean" S-70 configuration of 26.2 ft^2 to approximately 90 ft^2. This result shows the potentially significant BVI noise reduction that can be achieved by the *X*-force control concept.

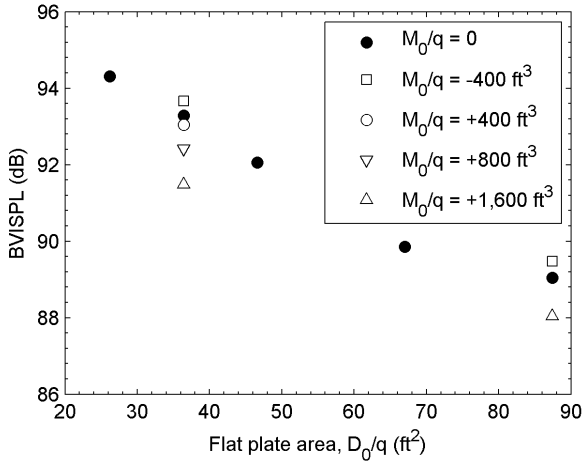

Figure 3. Effect of flat plate area and pitching moment on peak BVI noise

The SPL of the BVI noise that is radiated toward the ground by the baseline configuration (f = 36.4 ft^2) is shown in Figure 4. Figure 4 shows a projection contour plot of the BVI SPL computed by PSU-WOPWOP for a 500 ft radius hemispherical observer grid (white dots), centered at the rotor hub and aligned with the inertial frame of reference. Elevation angles are measured downward, from the horizon plane.

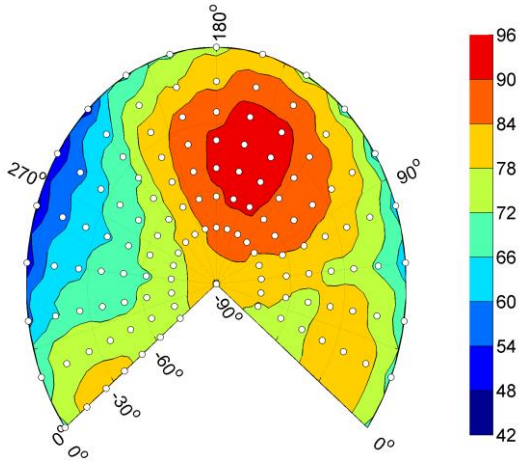

Figure 4. Baseline (f = 36.4 ft^2) BVI SPL at 500 ft

Generally, the peak BVI SPL direction did not vary. Peak BVI SPL was computed for the observer located along an azimuth of 140 deg and an elevation of 37.5 deg below the flight path vector. Only for f = 87.4 ft^2 (Figure 5) did the peak BVI SPL show a slight (downward) shift. The peak BVI SPL for f = 87.4 ft^2 was computed for the observer located at an azimuth of 120 deg and of elevation 50 deg.

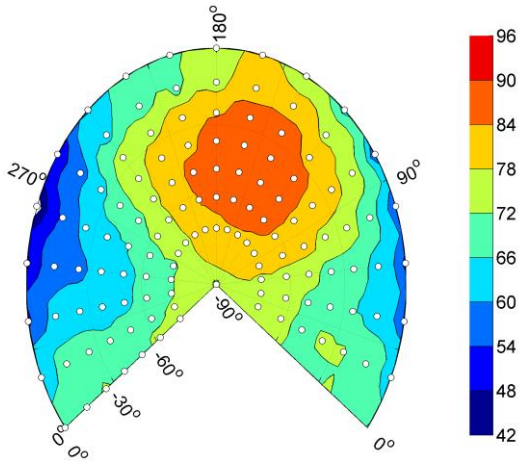

Figure 5. BVI SPL at 500 ft for f = 87.4 ft^2

Effect of Fuselage Pitching Moment. Figure 3 also shows the effect of varying pitching moment on BVI noise radiation, where reductions in the peak BVI SPL were obtained for increasingly larger nose-up (positive) pitching moments. Conversely, negative (nose-down) fuselage pitching moment variations resulted in peak BVI noise levels increasing relative to the baseline case. The minimum peak BVI SPL value obtained was approximately 91.5 dB, for M_0/q=1,600 ft^3, corresponding to a moderate 1.8 dB reduction relative to the baseline (93.3 dB).

The total BVI SPL radiated for M_0/q=1,600 ft^3 is shown in Figure 6. A very slight reduction in the BVI noise radiated is observed relative to the baseline (Figure 4).

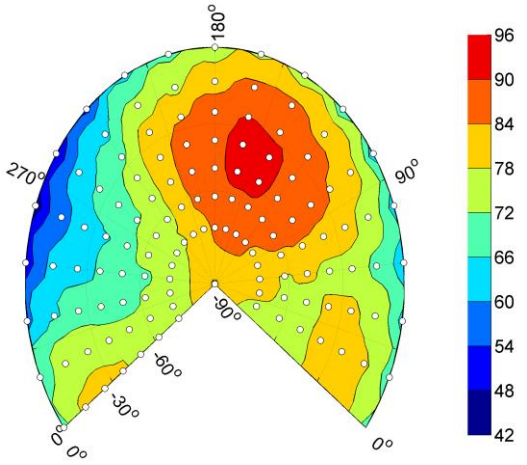

Figure 6. BVI SPL at 500 ft for M_0/q=1,600 ft^3 (f=36.4 ft^2)

Combined Effect. The overall effect of the pitching moment on the peak BVI SPL was slightly diminished at high drag levels (Figure 3), although the same general trends were observed. Increasing the nose-up pitching moment of the fuselage for the high drag configuration caused a 1 dB reduction in the peak BVI noise (from 89 to 88 dB) compared to the baseline configuration.

The total reduction, relative to the baseline, that was achieved by combining the changes in the two parameters was approximately 5.3 dB (6.3 dB relative to the 26.2 ft^2 configuration). The maximum combined effect on the overall noise radiated is illustrated in Figure 7.

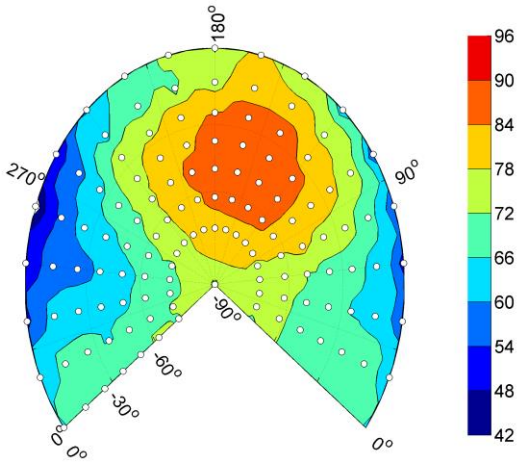

Figure 7. BVI SPL at 500 ft for FPA=87.4 ft^2 and M_0/q=1,600 ft^3

SPL Differences

The "global" effect of fuselage drag on BVI noise is illustrated in Figure 8 and Figure 9. Figure 8 highlights the effect of decreasing and increasing fuselage drag, relative to the baseline value. Reducing the drag (Figure 8a) caused notable increases of the BVI noise radiated downward and laterally towards the sides (both in the retreating and advancing blade sides). Increasing fuselage drag (Figure 8b) had the opposite effect, i.e., to decrease the SPL of the BVI noise radiated in the same general directions. Towards the front of the helicopter, where peak BVI is being radiated, the net effect is not as large, but a 1 dB reduction was still achievable for a ~10 ft^2 increase in flat plate area.

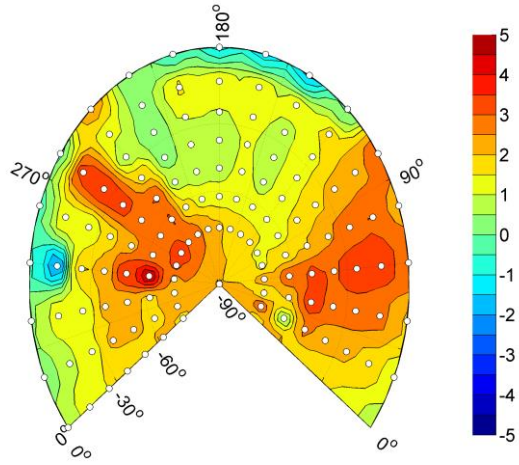

(a)

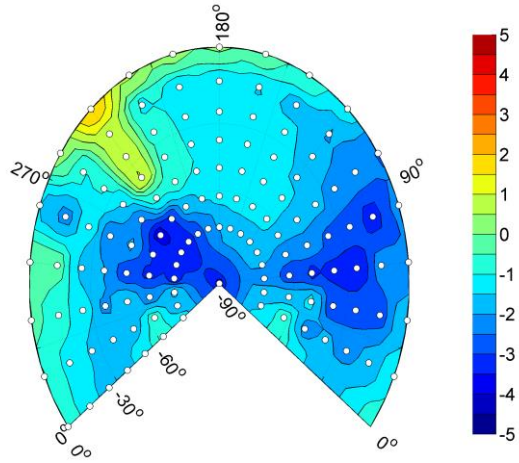

(b)

Figure 8. BVI SPL difference relative to the baseline (f=36.4 ft^2): (a) f=26.2 ft^2, and (b) f=46.6 ft^2

For larger fuselage drag changes, a region of increasing BVI noise was seen to form and develop near an azimuth of 240 deg (Figure 9). Simultaneously, the maximum reduction was identified to occur in a direction almost diametrically opposite (20-60 deg azimuth), with the peak located at an elevation between 10 and 30 deg below the horizon.

The locations of maximum BVI noise increase and decrease occur away from the peak baseline BVI and therefore have a negligible effect on the peak (Figure 5).

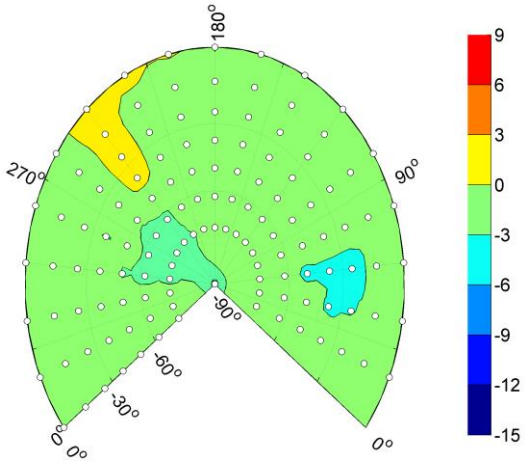

(a)

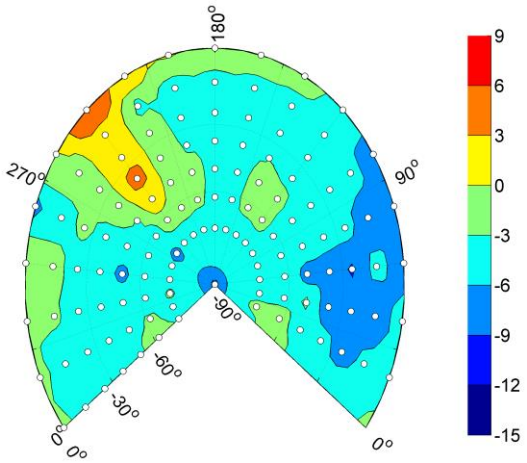

(b)

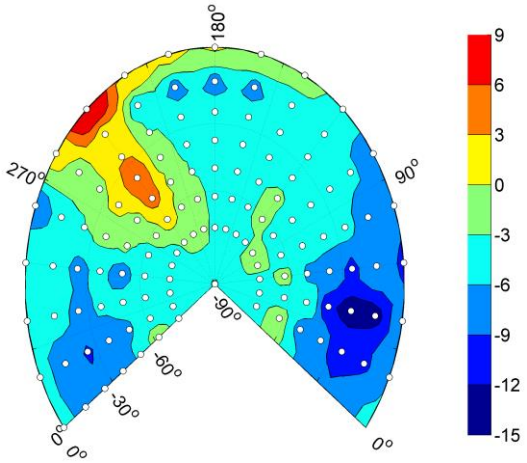

(c)

Figure 9. BVI SPL difference relative to the low drag fuselage (a) f=46.6 ft^2, (b) f=67.9 ft^2, and (c) f=87.4 ft^2

The effect of varying the pitching moment on BVI noise is illustrated in Figure 10. Generally, a region of increased BVI formed on the retreating blade side (azimuth 240-270 deg), for small elevation angles below the horizon (0-25 deg). In the region where BVI noise radiation is highest (120-180 deg azimuths), increasing the fuselage moment resulted in slightly larger reductions of BVI noise, with the maximum reduction for M_0/q=1,600 ft^3. Negative pitching moments generally resulted in slight increases of the BVI noise radiated. Positive pitching moments resulted in slight reductions of BVI noise SPL radiated in this same direction.

The observed trends were not absolute, however. Results for M_0/q=400 ft^3, for example, show much less pronounced differences in the BVI noise. Accordingly, there was a less pronounced increase on the retreating blade side, and a similarly attenuated reduction on the advancing blade side.

Rotorcraft Trim

Effect of fuselage drag. Results from the parametric sweep of the fuselage flat plate area (Figure 11) illustrate the net effect of drag on the vehicle and rotor trim angles. Crucially, highlighting the potential impact on BVI, the rotor was shown to tilt forward by a total of 3.85 deg in order to satisfy the propulsive trim requirement. This change in the rotor angle of attack was achieved primarily through the reorientation of the helicopter pitch attitude, since the pitching moment remained largely invariant.

Effect of fuselage pitching moment. The helicopter pitched increasingly upwards, in order to ensure propulsive trim force equilibrium (Figure 12). This was evidenced by the simultaneous forward tilt of the rotor disk relative to the body axis, and the negligible changes in the TPP aerodynamic angle of attack. Forward longitudinal cyclic would have had to be increased proportionally to compensate for the increased fuselage pitching moment, and thus maintain the moment equilibrium in pitch. The increasing nose-down (negative) hub pitch moment to compensate for the positive fuselage aerodynamic moment changes is shown in Figure 13. In response to this control input, the rotor TPP tilted forward, relative to the fuselage. However, the aerodynamic angle of attack of the rotor TPP remained approximately invariant, as evidenced in Figure 12, in order maintain the propulsive force equilibrium in trim.

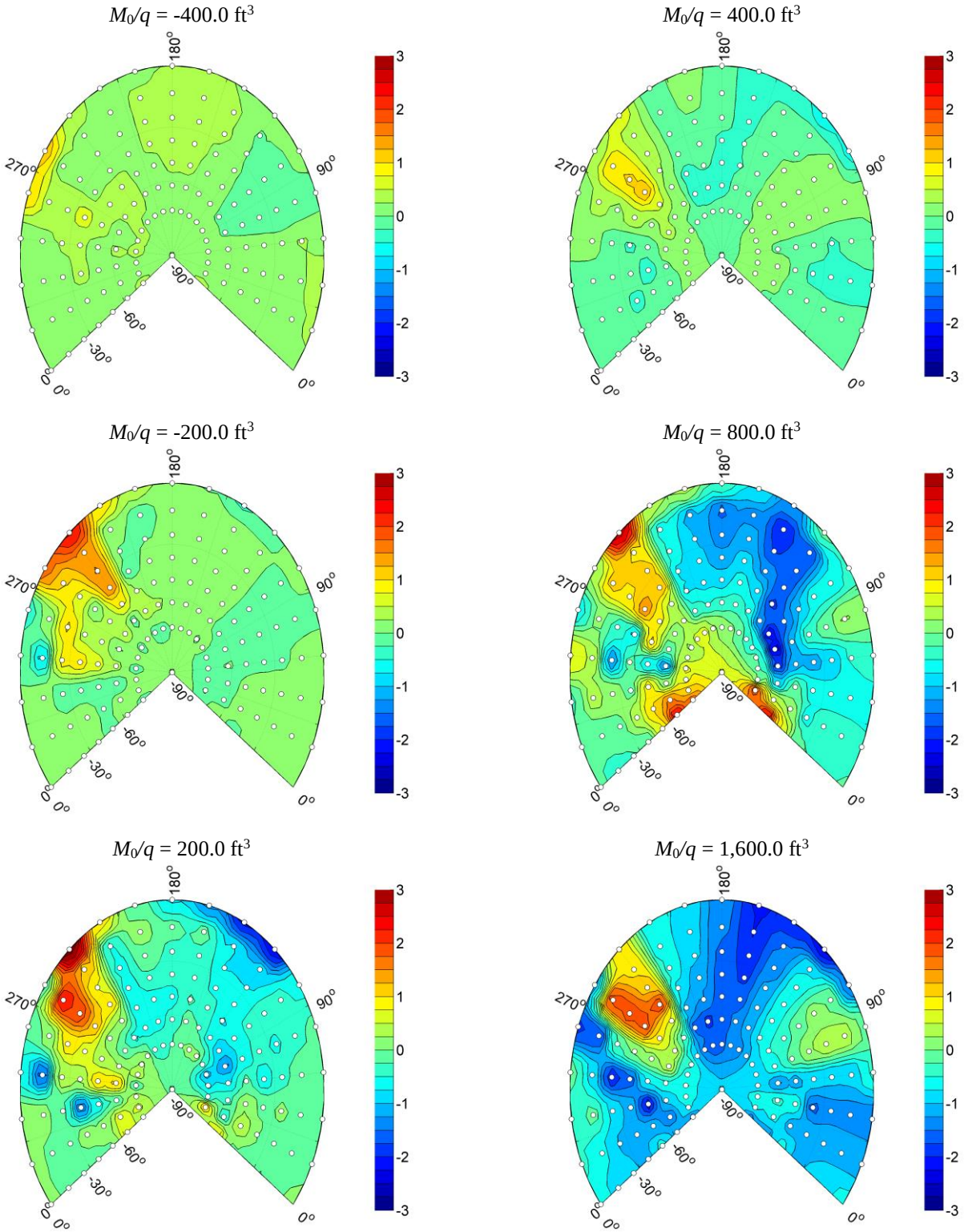

Figure 10. BVI SPL difference (dB) relative to baseline (M_0/q = 0 ft^3); f=36.4 ft^2

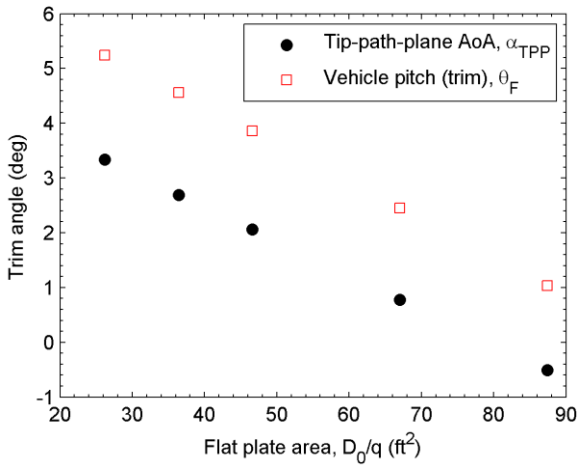

Figure 11. Effect of flat plate area on vehicle trim

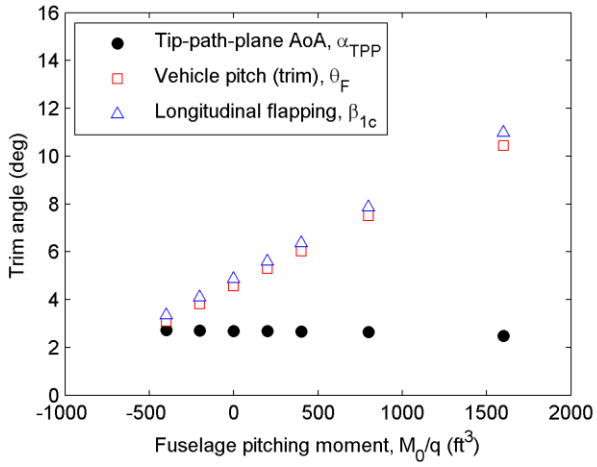

Figure 12. Effect of fuselage pitching moment on trim

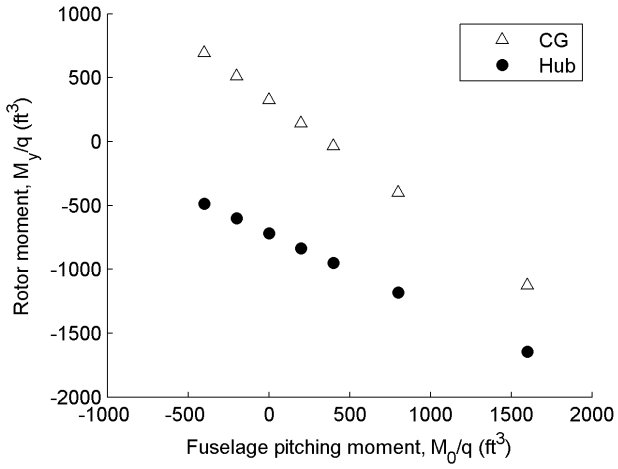

Figure 13. Rotor pitching moment in trim

DISCUSSION

The combined application of fuselage drag and positive pitching moments resulted in improved reductions of the peak BVI noise that was radiated by the rotor. This result was made possible by yet unidentified "second-order" effects of the pitching moment on the airloads. The changes in the pitching moment carried by the rotor likely caused a distortion of the wake geometry and changes to the blade tip vortex strength. This hypothesis has yet to be investigated.

Large changes in attitude were encountered for relatively small BVI noise reductions, which questions the practicability of these concepts for noise control. The fact that pitching moment and drag have opposing effects on the vehicle pitch in trim is a highly favorable characteristic, however. This allows the aircraft trim changes to be offset when simultaneously increasing the fuselage drag and pitching moment. More crucially, for this particular case, the cyclic control inputs were taken to the extents of their practical range, highlighting the potential control authority limitations of such a system.

On this evidence alone, the benefit of a noise control system relying solely on the use of pitching moment is questionable. The underlying mechanisms for the BVI noise reduction that was achieved in response to the pitching moment variations must be better understood before the concepts demonstrated in this study can be discounted or adopted for use in the practical design of flight control technologies for noise reduction.

CONCLUSIONS

Results from the comprehensive analysis and acoustics predictions lead to the following conclusions:

1. Fuselage drag was confirmed as an effective parameter for BVI noise control. Changes to fuselage drag cause the reorientation of the rotor tip-path-plane with respect to the airflow.

2. Varying the fuselage pitching moment causes small changes in the peak BVI noise radiated. The underlying mechanisms are not yet understood.

3. The independent effects of fuselage drag and pitching moment can be combined to achieve larger overall reductions in the peak BVI noise.

REFERENCES

[1]Jacklin, S. A. et al., "Full-Scale Wind Tunnel Test of an Individual Blade Control System for a UH-60 Helicopter," American Helicopter Society 58th Annual Forum, Montreal, Canada, June 11-13, 2002.

[2]Sim, B. W., JanakiRam, R. D., and Lau, B. H., "Reduced In-Plane, Low Frequency Noise of an Active Flap

Rotor," American Helicopter Society 65th Annual Forum, Grapevine, TX, May 27-29, 2009.

[3]Schmitz, F. H., "Reduction of Blade-Vortex Interaction (BVI) Noise Through X-Force Control," NASA TM-110371, September 1995.

[4]Schmitz, F. H., Gopalan, G., and Sim, B. WC., "Flight-Path Management/Control Methodology to Reduce Helicopter Blade–Vortex Interaction Noise," *Journal of Aircraft*, Vol. 39, (2), March-April 2002, pp. 193-205.

[5]Conner, D. A., Edwards, B. D., Decker, W. A., Marcolini, M. A., and Klein, P. D., "NASA/Army/Bell XV-15 Tiltrotor Low Noise Terminal Area Operations Flight Research Program," *Journal of the American Helicopter Society*, Vol. 47, (4), October July 2002, pp. 219-232.

[6]Johnson, W., "Rotorcraft Aerodynamics Models for a Comprehensive Analysis," American Helicopter Society 54th Annual Forum, Washington, DC, May 20-22, 1998.

[7]Shirey, J. S., Brentner, K. S., and Chen, Hn., "A Validation Study of the PSU-WOPWOP Rotor Noise Prediction System," 45th AIAA Aerospace Sciences Meeting and Exhibit, Reno, NV, January 8-11, 2007.

[8]Farassat, F., "Derivation of Formulations 1 and 1A of Farassat," NASA/TM-2007-214853, March 2007.

[9]Sim, B. WC. and Schmitz, F. H., "Blade-Vortex Interaction (BVI) Noise: Retreating Side Characteristics," Proceedings of the American Helicopter Society (AHS) Aeromechanics Specialists' Meeting, Atlanta, GA, November 13-14, 2000.

[10]Kitaplioglu, C., "Aeroacoustic Test of a Full-Scale UH-60 Main Rotor in the NASA Ames 80- by 120-Foot Wind Tunnel," NASA/TM - 2006 - 213487, August 2006.

[11]Yeo, H., Bousman, W. G., and Johnson, W., "Performance Analysis of a Utility Helicopter with Standard and Advanced Rotors," *Journal of the American Helicopter Society*, Vol. Vol. 49, (No. 3), July 2004, pp. 250-270.

[12]Kufeld, R. M. et al., "Flight Testing the UH–60A Airloads Aircraft," American Helicopter Society 50th Annual Forum, Washington, DC, May 11-13, 1994.

[13]Bousman, W. G. and Kufeld, R. M., "UH-60A Airloads Catalog," NASA/TM-205-212827, August 2005.